
**Separation Science and Technology**
Publication details, including instructions for authors and subscription information:
http://www.informaworld.com/smpp/title~content=t713708471

# Separation of Hydrogen-Lean Mixtures for a High-Purity Hydrogen by Vacuum Swing Adsorption

A. Kapoor[a]; R. T. Yang[a]
[a] DEPARTMENT OF CHEMICAL ENGINEERING, STATE UNIVERSITY OF NEW YORK AT BUFFALO, BUFFALO, NEW YORK

**To cite this Article** Kapoor, A. and Yang, R. T.(1988) 'Separation of Hydrogen-Lean Mixtures for a High-Purity Hydrogen by Vacuum Swing Adsorption', Separation Science and Technology, 23: 1, 153 — 178
**To link to this Article: DOI:** 10.1080/01496398808057640
**URL:** http://dx.doi.org/10.1080/01496398808057640

SEPARATION SCIENCE AND TECHNOLOGY, **23**(1-3), pp. 153-178, 1988

# Separation of Hydrogen-Lean Mixtures for a High-Purity Hydrogen by Vacuum Swing Adsorption

A. KAPOOR and R. T. YANG

DEPARTMENT OF CHEMICAL ENGINEERING
STATE UNIVERSITY OF NEW YORK AT BUFFALO
BUFFALO, NEW YORK 14260



**Abstract**

High-purity hydrogen is commercially produced by pressure swing adsorption from hydrogen-rich mixtures. In this work, a vacuum pressure swing adsorption cycle is used to produce high purity hydrogen from a hydrogen-lean binary mixture (20/80 $H_2$/CO) using zeolite 5A as the sorbent. The effects of different process variables on separation performance have been studied. The purity of hydrogen product increases at low throughput, high feed pressure, high end pressure of cocurrent depressurization, low end pressure of countercurrent evacuation, and short cycle time. Also, it was found that for a $H_2$-lean mixture, the separation is improved at higher ambient temperature. In addition, a new "vacuum purge" step was found to improve the separation and is therefore a promising step for commercial application.

## INTRODUCTION

Pressure swing adsorption (PSA) is one of the most important gas separation processes employing adsorption phenomenon. It has been widely used in air drying, air separation, octane improvement, and $H_2$ purification (*9, 14–16, 19, 20*). The principle underlying the PSA process is the fact that the adsorption amounts on various adsorbents increase with the gas partial pressure. Thus the adsorbent can be regenerated by rapidly reducing the partial pressure of adsorbed component. This is achieved either by lowering the total pressure or by using a purge gas. Since the initial development of PSA in 1960, many more sophisticated PSA processes have been developed and commercialized. The main steps

in a PSA cycle involve pressurization, purified product removal during a high-pressure feed step, and desorption during the blowdown (depressurization) step. Vacuum desorption has been used in some PSA processes involving a strong adsorbate (*18*). These PSA processes have been reviewed by Keller (*15*), Cassidy and Holmes (*14*), Wankat (*5*), and Yang (*9*).

Hydrogen purification remains the largest application of PSA. The demand for high purity hydrogen (over 99.999% purity) has been steadily increasing by the electronic industry and other industries. The commercial PSA processes, however, can produce a high purity $H_2$ at a high recovery only from a $H_2$-rich (over 70%) feed. In this paper we report a PSA cycle which can produce high purity $H_2$ at high recoveries from a $H_2$-lean mixture. A 20/80 $H_2$/CO mixture was used as the feed. Such a mixture was chosen because similar mixtures are available from many industrial processes such as coal gasification.

In the present work an attempt has been made to study the PSA separation of a 20/80 $H_2$/CO mixture. The effects of different process variables such as feed pressure, throughput, end pressure of cocurrent depressurization, end pressure of countercurrent evacuation, and cycle time on separation performance have been determined. In addition, the benefits of a new "vacuum purge" step have been investigated. Also, an answer has been given to the question of the effect of ambient temperature on PSA process. An equilibrium model was developed to simulate the PSA process. The model simulation results are in fair agreement with the experimental data.



## PROCESS DESCRIPTION

The PSA process used in this study consisted of the following four steps in each cycle.

Step I: $H_2$ pressurization
Step II: High pressure adsorption
Step III: Cocurrent depressurization
Step IV: Countercurrent evacuation

Two or more interconnected beds are operated synchronously, so continuous feed and products are possible.

In Step I the bed is pressurized to the feed pressure by $H_2$ since pressurization by the lighter component gives better separation (*1*). In Step II the high-pressure feed flows through the column while the

effluent from the bed is taken as $H_2$ product. Cocurrent depressurization, Step III, is used to recover $H_2$ remaining in the voids. In Step IV the bed is evacuated from the feed end. The evacuation serves to clean the bed so high purity $H_2$ product is possible.

The performance of a PSA process is judged by three separation results: product purity, product recovery, and throughput, all at cyclic steady-state. The effluents from Steps II and III are collected as $H_2$ product, and that from Step IV as CO product. The product purity is defined as the volume averaged concentration over the entire product, and is expressed as vol%. The throughput is defined as the total feed volume (L STP) treated per unit time per unit weight of sorbent (L STP/h/kg). The product recoveries are defined as:

$$\text{CO recovery} = \frac{\text{CO from Step IV}}{\text{CO in feed (in Step II)}}$$

$$H_2 \text{ recovery} = \frac{(H_2 \text{ from Step II and Step III}) - (H_2 \text{ used in Step I})}{H_2 \text{ in feed (in Step II)}}$$

## EXPERIMENTAL

### Apparatus

The schematic diagram of the apparatus has been shown elsewhere (*3*, *6*). The single column apparatus was designed in this laboratory to simulate all steps in the PSA cycle. The adsorption column was packed with 608 g commercial 5A zeolite. Table 1 shows the sorbent and bed characteristics. Four solenoid valves located at the feed, cocurrent, countercurrent, and high-pressure $H_2$ lines were used to regulate the flow directions of different streams. These four solenoid valves were hooked to an electronic timer. The pressure history of the process was recorded by using a pressure transducer connected at the bottom ($H_2$ product) end of the column. A vacuum gauge connected to the vacuum line was used to record the pressure history during the countercurrent evacuation step. The temperature history of the bed was recorded at three locations in the bed (15 cm from the top end, in the middle, and 15 cm from the bottom end of the column). Gas samples were taken from two sampling ports (one in the cocurrent and the other one in the countercurrent line) which were fitted with septa by syringes. A mechanical vacuum pump was used for the evacuation step.

TABLE 1
Adsorption Bed Characteristics

| | |
|---|---|
| Bed inside radius | $r = 2.05$ cm |
| Bed length | $L = 60$ cm |
| Pellet size | $d = 0.158$ cm |
| Bulk density | $\zeta = 0.77$ g/cm$^3$ |
| Pellet density | $\zeta_p = 1.14$ g/cm$^3$ |
| Total void fraction | $\varepsilon = 0.756$ |
| Heat capacity of zeolite | $C_{ps} = 0.92$ J/g/°C |
| Heat capacity of wall | $C_{pw} = 0.46$ J/g/°C |

The gases used in experiments were obtained from Linde, Union Carbide. The feed mixture containing 20% $H_2$ and 80% CO (by volume) was premixed. The $H_2$ used for bed pressurization was ultrahigh purity grade at 99.999% minimum.



## Procedure

Prior to the start of an experiment, the bed was regenerated at 300°C in helium for 24 h.

A typical PSA run was carried out as follows: The timer was programmed for the required cycle timings and Step I was initiated by opening the solenoid valve connected to the high-pressure $H_2$. The column pressure was controlled by adjusting the pressure regulator connected to the gas tank and the flow rate by adjusting the fine needle valve. The high-pressure adsorption (Step II) started when the solenoid valve connected to the feed line and cocurrent line were opened simultaneously by the timer. The flow rate in Step II was controlled by adjusting a needle valve on the cocurrent line. Step III, cocurrent depressurization, was achieved by closing the solenoid valve on the feed line. The flow rate in this step was adjusted to get the required end pressure of this step. The cocurrent line solenoid valve was closed and the countercurrent line valve was opened simultaneously to achieve Step IV.

A cyclic steady-state was generally reached after 8 cycles from startup with a clean bed. After the steady-state was achieved, a complete set of flow rates and product samples (every 15 to 30 s) was taken.

The samples were later analyzed using a GC. A molecular sieve 5A column (6 ft by ¼ in., 80/100 mesh) was used with argon as the carrier gas. The samples could be analyzed with an accuracy of 10 ppm. The

reproducibility of these measurements was found to be good by repeated analysis of standard samples. The standard deviation was less than 3% of the mean.

Experiments were performed to study the effects of throughput (28–58 L STP/h/kg), feed pressure (200–400 psig), end pressure of Step III (0–30 psig), and cycle time (8–16 min) on separation. The effects of end pressure of Step IV (1–15 psia) and ambient temperature (5–35°C) were studied by computer simulation runs. A new process step (vacuum purge) was also studied, i.e., the effect of purge/feed ratio by vacuum purge on separation.

## THEORETICAL ANALYSIS

In order to develop a mathematical model for this system, the following simplifying assumptions and approximations were made:

1. The ideal gas law applies.
2. The axial pressure gradient is neglected.
3. Thermal equilibrium is assumed between the fluid and the particles.
4. No variation exists in the radial direction for both concentration and temperature.
5. The flow pattern is described by an axial dispersed plug flow model.



This model is similar to our previous models (*3*, *4*, *6*) except that an axial dispersion term is included. With these assumptions and approximations the process can be described by the following set of equations.

The total material balance in the column can be written

$$-D\frac{\partial^2 C}{\partial z^2} + \frac{\partial}{\partial z}(uC) + \frac{\partial C}{\partial t} + \frac{(1-\varepsilon)}{\varepsilon}\frac{\partial q}{\partial t} = 0 \tag{1}$$

Material balance for Component $i$:

$$-D\frac{\partial^2 C_i}{\partial z^2} + \frac{\partial}{\partial z}(uC_i) + \frac{\partial C_i}{\partial t} + \frac{(1-\varepsilon)}{\varepsilon}\frac{\partial q_i}{\partial t} = 0 \tag{2}$$

where $C_i = Py_i/RT$.

If the resistance to mass transfer is negligible (equilibrium model), we have

$$\partial q/\partial t = \partial q^*/\partial t \tag{3}$$

Energy balance in the column is given by

$$\frac{\partial}{\partial z}(uCC_pT) + \frac{\partial}{\partial t}(CC_pT) + \frac{(1-\varepsilon)}{\varepsilon}\frac{\partial}{\partial t}[q(C_{pa}T - H)] + \frac{(1-\varepsilon)}{\varepsilon}$$

$$\times \frac{\partial}{\partial t}(C_{ps}T) + \frac{2h}{r}(T - T_w) = 0 \tag{4}$$

where the heat of adsorption is

$$H = \sum_{i=1}^{N} x_i H_i \tag{5}$$

and the heat capacities are

$$C_p = \sum_{i=1}^{N} y_i C_{pi} \tag{6}$$

$$C_{pa} = \sum_{i=1}^{N} x_i C_{pai} \tag{7}$$

$$C_{pi} = A_i + B_i T + C_i T^2 + D_i T^3 \tag{8}$$

The parameters for Eq. (8) are listed in Table 2a.

The last term in Eq. (4) is necessary because, in the experimental unit, the diameter of the bed is small and the heat transferred to the surroundings as well as the heat capacity of the wall cannot be neglected. So the temperature of the wall is given by

$$2\pi rh(T - T_w) = \zeta_w C_{pw} A_w \frac{\partial T_w}{\partial t} + 2\pi h_0 (T_w - T_0) \tag{9}$$

TABLE 2a
Parameters for Heat Capacities

| | $A$ | $B \times 10^3$ | $C \times 10^6$ | $D \times 10^9$ |
|---|---|---|---|---|
| $H_2$ | 6.483 | 2.215 | −3.289 | 1.826 |
| CO | 7.373 | −3.07 | 6.662 | −3.037 |

## INITIAL AND BOUNDARY CONDITIONS

The model computation was started at the end of Step I (hydrogen pressurization). So at the initial condition of $t = 0$, the column was pressurized to the feed pressure by hydrogen.

### Initial Conditions

$P = P_f$, $T = T_0$, $q = q_0$ at $t = 0$ and $0 < z < L$:

$$y_{H_2} = x_{H_2} = 1.0 \tag{10}$$

$y_i = x_i = 0$ for $i = \text{CO}$ at $t = 0$ and $0 < z < L$.



### Boundary Conditions

The boundary conditions of the ensuing cycle are:

*Step II. High-pressure adsorption:*

$$\text{at } z = 0: \qquad y_i = y_f \,(\text{or } C_i = C_f)$$

$$T = T_0$$

$$\text{at } z = L: \qquad \left.\frac{\partial C}{\partial z}\right|_{z=L} = 0, \qquad u = u_{\text{out}} \tag{11}$$

*Step III. Concurrent depressurization:*

$$\text{at } z = 0: \qquad u = 0$$

$$y_i = y_f$$

$$\text{at } z = L: \qquad \left.\frac{\partial C}{\partial z}\right|_{z=L} = 0 \tag{12}$$

*Step IV. Countercurrent evacuation:*

$$\text{at } z = 0: \qquad \left.\frac{\partial C}{\partial z}\right|_{z=0} = 0 \tag{13}$$

$$\text{at } z = L: \quad u = 0$$

$$y_i = y_{\text{end of Step III}}$$

*Step I. Hydrogen pressurization:*

$$\text{at } z = 0: \quad u = 0,$$

$$y_i = y_{\text{end of Step IV}}$$

$$\text{at } z = L: \quad y_i = 1.0 \text{ for } i = H_2 \tag{14}$$

$$y_i = 0.0 \text{ for } i = CO$$

The pressure history $P = P(t)$ was an input variable in PSA.

The initial conditions for each step are the conditions (concentration and temperature profiles in the column) at the end of the preceding step.



## INPUT TO THE MODEL

Single gas adsorption isotherms for $H_2$ and CO were measured on Molecular Sieve 5A in this laboratory and were correlated by a Langmuir-type fit. The equilibrium adsorption data for the mixture were calculated using the Loading Ratio Correlation (LRC). LRC was chosen because of its noniterative nature which can reduce the amount of computation. LRC is given by

$$q_i^* = \frac{q_{mi} b_i P_i}{1 + \sum_{i=1}^{N} b_i P_i} \tag{15}$$

where $q_{mi} = a_i + b_i/T$

$b_i = \exp(c_i + d_i/T)$

$P_i = Py_i$

The parameters for Eq. (15) are listed in Table 2b.

Isosteric heats of adsorption were also calculated from the experimental isotherms. The heats of adsorption were assumed constant over the range of conditions of our study, thus average values were used in the model. These values are also listed in Table 2b. A constant value of

TABLE 2b
Parameters for LRC Equation and Heats of Adsorption

| | LRC Parameters | | | | |
|---|---|---|---|---|---|
| | *a* | *b* | *c* | *d* | H (J/mol) |
| $H_2$ | −3.138 | 1,652.4 | −5,234 | 118.12 | 10,032 |
| CO | 0.235 | 862.0 | −5.920 | 1262.3 | 22,990 |

overall heat transfer coefficient, which accounted for the insulation layer and free convection, with the resistance in the insulation layer being dominant, was used in the model. The value was taken to be (*6*)

$$9.58 \times 10^{-5} \text{cal/cm}^2/^\circ\text{C/s}$$

The value of the wall heat transfer coefficient $h_0$ used (*3*) was

$$3.0 \times 10^{-3} \text{cal/cm}^2/^\circ\text{C/s}$$

The pressure history $P(t)$ data from the transducer/recorder were fitted into polynomials (for each step), which were then used as the boundary conditions.

The values of the axial dispersion coefficient, $D$, were calculated using (*7*):

$$\frac{1}{N_{\text{Pec}}} = \frac{0.3}{G} + \frac{0.5}{1 + (3.8/G)} \tag{16}$$

where

$$G = N_{\text{Re}} N_{\text{Sc}}$$

and

$$N_{\text{Pec}} = ud_p/D$$

It was found that the effect of axial dispersion on the results was insignificant. The calculated values of the Peclet number, defined as $uL/D$, where $L$, the length of the adsorber bed, were much higher than 100. A similar observation has also been reported in the literature (*3*, *8*).

## NUMERICAL SOLUTION OF MODEL

An implicit backward finite difference method was used to solve Eqs. (1), (2), and (4) combined with Eqs. (3) and (5)–(9). The computation was initiated by assuming a set of values for $y_i$ and $T$. Equation (15) was then used to calculate $q_i$ and $x_i$. Then Eqs. (1), (2), and (4) were solved for $u$, $y_i$, and $T$. The iteration was continued until $y_i$ was within $10^{-6}$ and temperature $T$ was within $10^{-3}$ of the assumed value. In a typical computation, 30 space steps and 1920 time steps were used for each PSA cycle. The model was always stable and convergent in the range of conditions used in this study. All computation was performed on a VAX-780 computer. It took approximately 100 s CPU time for each cycle, and it generally took 8 cycles to reach cyclic steady-state.



## RESULTS AND DISCUSSION

In our earlier experiments it was found that for a hydrogen-lean mixture (20% $H_2$, 80% CO) the conventional 5-step cycle [including purge step (*2*, *3*, *9*)] gives low hydrogen recovery. The reason is that an appreciable amount of $H_2$ purge compared to the amount of $H_2$ in the feed (high purge/feed ratio) has to be used to get a high-purity $H_2$ product in Step II. In this study the purge step was replaced by an evacuation step (the evacuation step was combined with the countercurrent blowdown step) to improve the hydrogen recovery.

The experimental goal of this study was to produce a high-purity $H_2$ product (99.999% by volume) from a mixture of 20/80 $H_2$/CO and study the effects of operating variables on separation. When comparing the results of different runs, it should be kept in mind that all runs were designed to produce high-purity $H_2$ in Step II.

In a multibed PSA process (typical commercial operation) the bed is pressurized (Step I) by the effluents from Step II and some portion of effluents from Step III. In the literature (*10*) it has been shown that the purity of $H_2$ product from Step II is limited by the purity of $H_2$ used for pressurization and purge (if any) for a multibed process. In such a process, the product from Step II should have a high purity. To simulate the multibed conditions in our experiments, the purity of Step II product was 99.999% and the purity of $H_2$ used for Step I was also 99.999%. (This was also the experimental condition.) The $H_2$ recovery was defined by assuming that all the effluents from Steps II and III were either products or could be internally used for repressurization. But in some experiments where the purity of Step III product is low, the above assumption may not

be very good. In such cases the actual recovery in a commercial operation would be lower than predicted by our definition.

## COMPARISON BETWEEN THEORY AND EXPERIMENTS

The model discussed in the last section was used to predict the results of all runs. For all experimental data and model predictions, the main results were the instantaneous composition and flow rates of different product streams. From this data, the throughput, product purities, and product recoveries were calculated. The comparisons between experimental data and model predictions are given in Table 3 and Fig. 1 for a typical run (Run B). Table 3 lists the flow rates and mole percent of $H_2$ in the effluents of corresponding step, whereas Fig. 1 shows the CO mole percent ($H_2$ mol% = 100 − CO mol%) as a function of time and the pressure history for Run B (the same pressure history was used for the model). The quantitative comparison between the experiments and model predictions is fair, but the model is capable of predicting all the steps of PSA. The qualitative trends are predicted very well. The equilibrium model always predicted a steep wavefront and consequently better separation. Besides the inherent nature of the model (equilibrium assumption), possible causes for this discrepancy were: inaccuracies in the model inputs such as equilibrium isotherms, pressure history, and the assumption of neglecting the pressure drop across the column.

The temperature history predicted by the model was compared with the experimentally recorded temperature history. Figure 2 shows the comparison for a typical run (Run B) at three locations in the bed. The overall comparison is good. It was found that in Eq. (9) both terms on the right-hand side were important. For the small column used in this study, the heat capacity of the wall as well as the heat transfer with the surroundings affect the temperature in the column. The peaks in the top and middle curves correspond to the position of the CO wavefront. The curves show that the CO wavefront never touches the lower point in the column. It was found that it was very important to keep the product end of the bed clean in order to produce a high purity hydrogen product. The small hump in the lowest curve is probably due to the adsorption of hydrogen on the clean bed in Step I (bed pressurization was done from the bottom of the column).

## EFFECTS OF PROCESS VARIABLES ON SEPARATION

For a given gas mixture/adsorbent system, the process variables for the vacuum cycle are: throughput, feed pressure, end pressure of cocurrent

TABLE 3
Steady-State Experimental and Model Prediction Results for PSA Separation of a Feed of 20/80 $H_2$/CO

| Step | Time (s)[a] | $y_{H_2}$ (%) | | Effluent flow rate[b] | |
|---|---|---|---|---|---|
| | | Exptl | Equilibrium model | Exptl | Equilibrium model |
| II | 270 | 99.999 | 99.999 | 1.00 | 1.00 |
| | 330 | 99.999 | 99.999 | 1.00 | 1.00 |
| | 390 | 99.999 | 99.999 | 1.00 | 1.00 |
| | 450 | 99.999 | 99.999 | 1.00 | 1.00 |
| III | 510 | 99.999 | 99.999 | 4.03 | 3.57 |
| | 570 | 99.999 | 99.993 | 5.24 | 4.09 |
| | 630 | 99.999 | 99.951 | 4.41 | 3.48 |
| | 690 | 44.204 | 73.412 | 2.12 | 2.32 |
| IV | 750 | 4.717 | 4.600 | 2.09 | 1.71 |
| | 810 | 5.520 | 2.469 | 1.28 | 1.11 |
| | 870 | 4.789 | 2.143 | 0.92 | 1.06 |
| | 930 | 4.201 | 1.760 | 0.71 | 1.02 |

[a]From the beginning of Step I.
[b]Flow rate in L STP/min.



depressurization, end pressure of countercurrent evacuation, and cycle time. The effects of these variables on separation are discussed below.

## Effects of Throughput

Three runs (Runs A, B, and C) were made to study the effects of throughput. For a given bed (fixed amount of adsorbent) the effect of throughput can be studied by varying the feed rate. In Runs A, B and C, the feed rate was varied from 46.7 to 96.7 L STP/h while keeping the other process conditions the same. The separation results of these runs are compared in Table 4 and Fig. 3. It is clear that higher throughput results in lower purity of lighter component ($H_2$). On the other hand, it improves $H_2$ recovery and CO purity. These effects can be better analyzed in terms of bed utilization. Bed utilization is defined as the fraction of bed covered by the heavy component wavefront in Step II. As the feed rate increases, bed utilization also increases (and the fraction of clean bed decreases). This results in an early breakthrough (in Step III) and thus the purity of $H_2$ decreases. But early breakthrough helps recover more of the $H_2$ from the voids (in Step III), thus increasing the $H_2$ recovery, and also increases the ratio of CO/$H_2$ loading on the bed. Consequently, CO product purity is improved.

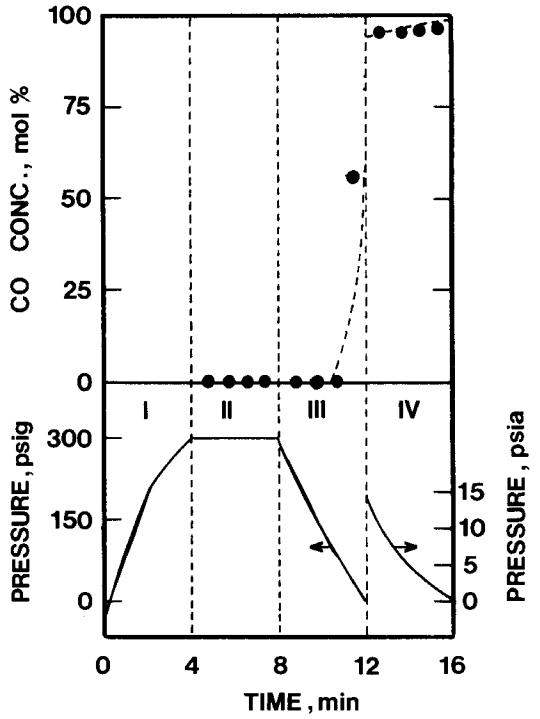


FIG. 1. Effluent concentration and pressure history at steady-state PSA for Run B. Points: experimental. Dashed curve: predicted.



The effects of throughput were well predicted by the model. Similar effects have been explained by Yang and Doong (*3*) for a 50/50 $H_2/CH_4$ mixture and by Cen and Yang (*2*) for a 50/50 $H_2/CO$ mixture on activated carbon. On comparison with their results it is clear that in our study the purity and recovery of $H_2$ are most sensitive to the feed rate. The reason for this is the low percentage of $H_2$ in the feed mixture. Hence, a small change in $H_2$ adsorption/desorption makes a large change in purity and recovery of the same component.

## Effects of Feed Pressure

Three runs (Runs G, B, and F) are compared in Table 4 and Fig. 4 to show the effects of feed pressure. The feed pressure was varied from 200 to 400 psig while keeping other process conditions nearly the same. From

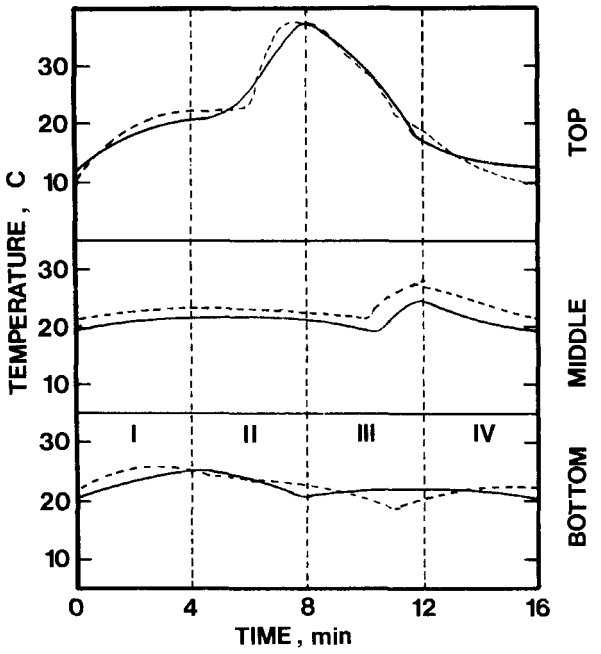


FIG. 2. Steady-state PSA temperature histories for Run B at three locations in the bed. Top (15 cm from feed end of bed), middle (30 cm from feed end), and bottom (45 cm from feed end). Solid line: experimental. Dashed line: predicted.



Table 4 and Fig. 4 it can be seen that a higher feed pressure was favorable for separation. The $H_2$ purity increased with an increase in feed pressure. According to Fig. 4, there is a discrepancy in the trends shown (for $H_2$ purity, Step III, as a function of feed pressure) by the model predictions, because the $H_2$ purity tends to level off at still higher pressures. Thus a feed pressure above 400 psig was not desirable because of the additional energy required. With other conditions fixed, an increase in feed pressure means lower bed utilization. From our earlier discussion on bed utilization and bed loading, the ratio of $CO/H_2$ bed loading would be low at higher feed pressures, and this would result in low CO product purity and low $H_2$ recovery.

### Effects of End Pressure of Cocurrent Depressurization

The cocurrent depressurization is a very important step for bulk separation. Three runs (Runs B, D, and E) were made to study the effects

TABLE 4
Cyclic Steady-State Results of PSA Separation of a 20/80 $H_2$/CO Mixture at Different Operation

| | Run | | | | | | | | | | | |
|---|---|---|---|---|---|---|---|---|---|---|---|---|
| | A | | B | | C | | D | | E | | F | |
| | Exptl | Calc | Exptl | Calc | Exptl | Calc | Exptl | Calc | Exptl | Calc | Exptl | Calc |
| Feed pressure, psia | 314.7 | | 314.7 | | 314.7 | | 314.7 | | 314.7 | | 414.7 | |
| End pressure, Step III, psia | 14.7 | | 14.7 | | 14.7 | | 32.7 | | 44.7 | | 14.7 | |
| End pressure, Step IV, psia | 1.0 | | 1.0 | | 1.0 | | 1.0 | | 1.0 | | 1.0 | |
| Cycle time, min | 16 | | 16 | | 16 | | 16 | | 16 | | 16 | |
| Purge/feed ratio | 0.0 | | 0.0 | | 0.0 | | 0.0 | | 0.0 | | 0.0 | |
| Throughput, L STP/h/kg | 28.031 | 27.141 | 46.512 | 42.713 | 58.737 | 58.367 | 46.812 | 45.519 | 46.419 | 44.844 | 45.975 | 44.422 |
| $H_2$ purity, Step II | 99.999 | 99.999 | 99.999 | 99.999 | 99.999 | 99.999 | 99.999 | 99.999 | 99.999 | 99.999 | 99.999 | 99.999 |
| $H_2$ purity, Step III | 99.999 | 99.999 | 92.519 | 95.411 | 84.151 | 88.363 | 93.552 | 98.209 | 99.999 | 99.999 | 98.019 | 98.112 |
| $H_2$ recovery | 42.363 | 54.743 | 83.606 | 89.071 | 97.695 | 97.665 | 44.926 | 49.012 | 11.111 | 21.101 | 70.564 | 83.814 |
| CO purity, Step IV | 87.396 | 89.841 | 95.136 | 97.008 | 99.207 | 99.697 | 86.361 | 88.679 | 81.812 | 83.525 | 92.612 | 95.829 |
| CO recovery | 99.999 | 99.999 | 80.148 | 85.545 | 73.201 | 76.547 | 87.183 | 90.468 | 99.999 | 99.999 | 92.234 | 92.684 |

*(continued)*

TABLE 4 (continued)

| | Run | | | | | | | | | |
|---|---|---|---|---|---|---|---|---|---|---|
| | G | | H | | I | | J | | K | |
| | Exptl | Calc | Exptl | Calc | Exptl | Calc | Exptl | Calc | Exptl | Calc |
| Feed pressure, psia | 214.7 | | 314.7 | | 314.7 | | 314.7 | | 314.7 | |
| End pressure, Step III, psia | 14.7 | | 14.7 | | 14.7 | | 14.7 | | 14.7 | |
| End pressure, Step IV, psia | 1.0 | | 1.0 | | 1.0 | | 1.0 | | 1.0 | |
| Cycle time, min[a] | 16 | | 16 | | 16 | | 16 | | 16 | |
| Purge/feed ratio | 0.0 | | 0.0 | | 0.11 | | 0.24 | | 0.24 | |
| Throughput, L STP/h/kg | 45.637 | 45.531 | 57.725 | 57.552 | 57.262 | 57.529 | 59.048 | 58.431 | 56.941 | 57.963 |
| $H_2$ purity, Step II | 99.999 | 99.999 | 99.999 | 99.999 | 99.999 | 99.999 | 99.999 | 99.999 | 99.999 | 99.999 |
| $H_2$ purity, Step III | 88.434 | 90.736 | 96.177 | 98.898 | 99.999 | 99.985 | 88.283 | 91.346 | 96.370 | 98.138 |
| $H_2$ recovery | 90.878 | 93.754 | 85.848 | 90.152 | 41.375 | 59.566 | 96.188 | 96.201 | 88.475 | 90.083 |
| CO purity, Step IV | 97.161 | 98.160 | 96.241 | 97.358 | 87.220 | 90.824 | 98.851 | 99.117 | 97.014 | 98.744 |
| CO recovery | 78.399 | 82.501 | 90.545 | 90.514 | 99.999 | 99.946 | 81.860 | 84.526 | 93.619 | 96.074 |

[a]For Runs H and I, Step IV was for 4 min.

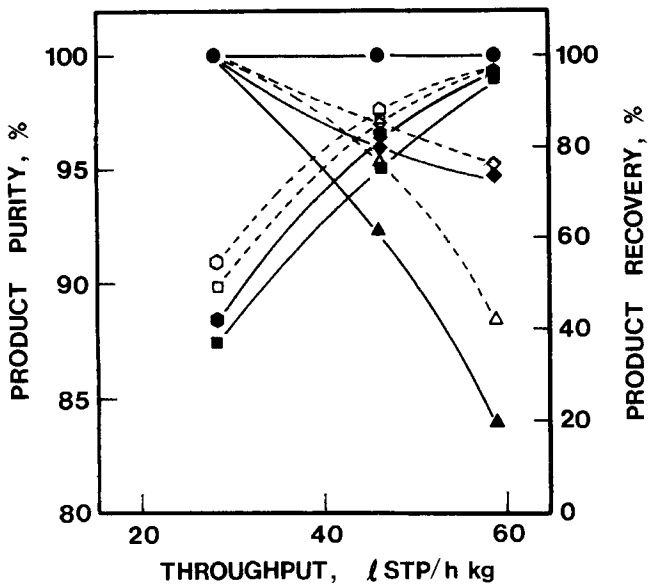


FIG. 3. Effects of throughput on PSA separation. (●) $H_2$ purity Step II, (▲) $H_2$ purity Step III, (■) CO purity Step IV, (⬢) $H_2$ recovery, (♦) CO recovery. Solid line: experimental. Dashed line: predicted.



of end pressure of this step. These three runs are compared in Table 4 and Fig. 5. It is clear that for $H_2$ purity and recovery, it is probably the most important parameter (especially for a $H_2$ lean mixture). The end pressure was varied from 0 to 30 psig while keeping all other conditions nearly the same. The higher cocurrent depressurization end pressure had the following effects: 1) to increase the $H_2$ product purity, 2) to decrease the CO product purity, and 3) to decrease the $H_2$ product recovery. The effects were so strong that an increase in end pressure of this step from 0 psig (Run B) to 30 psig (Run E) resulted in an increase in $H_2$ purity (Step III) from 92 to 99%, a decrease in $H_2$ recovery from 83 to 11%, and a decrease in CO purity (Step IV) from 95 to 82%.

The main function of this step was to increase the concentration of the strongly adsorbed component in the bed. It eluted the $H_2$ from the mass transfer zone, which was responsible for higher hydrogen recovery and increased CO purity. Since the adsorption isotherms of $H_2$ and CO on the molecular sieve are favorable, the wavefronts of these components broaden as the pressure is lowered (*9, 11*). Thus we see that lowering of

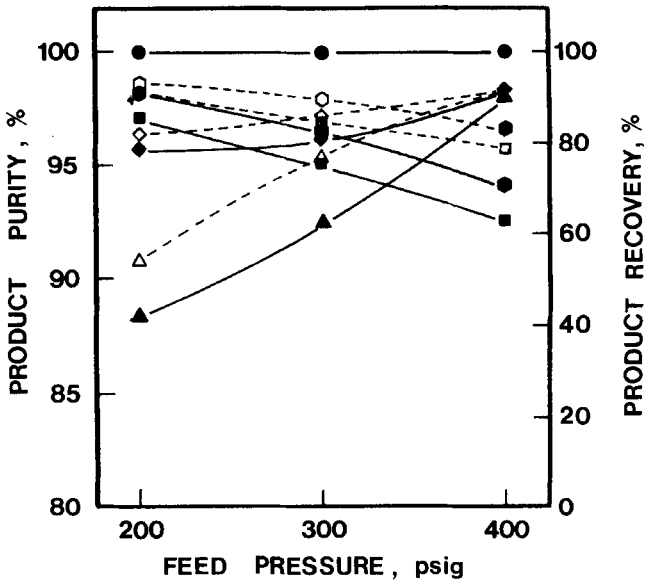


FIG. 4. Effects of feed pressure on PSA separation. (●) $H_2$ purity Step II, (▲) $H_2$ purity Step III. (■) CO Purity Step IV, (⬢) $H_2$ recovery, (♦) CO recovery. Solid line: experimental. Dashed line: predicted.



end pressure of Step III results in a more diffuse CO wavefront, causing more contamination of $H_2$ product.

### Effects of End Pressure of Countercurrent Evacuation

For the 4-step cycle used in this study (without the purge step), a lower end pressure of the countercurrent evacuation step means a cleaner bed and hence a higher purity $H_2$ product. Three modeling runs (Runs L, M and N) were made to show the effects of this parameter, and the separation results of these runs are compared in Table 5 and Fig. 6. It can be seen that a decrease in end pressure of Step IV resulted in higher $H_2$ purity but the purity of CO was lowered. The decrease in CO purity is due to the fact that more $H_2$ was eluted in Step IV as a consequence of lower pressure. Similar effects were reported (*4*, *12*) for cycles involving a purge step. It was concluded (*4*) that the purge/feed ratio required for a given purity of the light component decreases with a decrease in purge pressure. The conclusion is again a consequence of bed cleaning due to lower end pressure of the purge step.

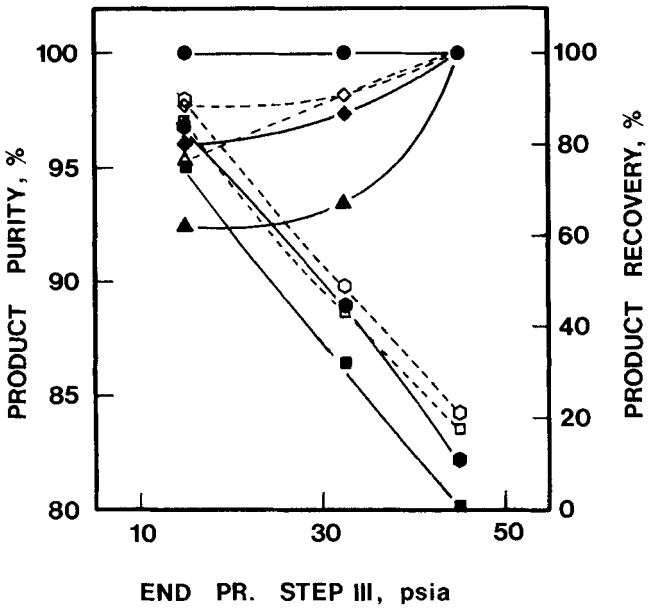


FIG. 5. Effects of end pressure of cocurrent depressurization step on PSA separation. (●) $H_2$ purity Step II, (▲) $H_2$ purity Step III, (■) CO purity Step IV, (⬢) $H_2$ recovery, (♦) CO recovery. Solid line: experimental. Dashed line: predicted.

TABLE 5
Effects of End Pressure of Countercurrent Evacuation (Step IV) on PSA Separation

| | Run | | |
|---|---|---|---|
| | L | M | N |
| Feed pressure, psia | 314.7 | 314.7 | 314.7 |
| End pressure, Step III, psia | 44.7 | 44.7 | 44.7 |
| End pressure, Step IV, psia | 1.0 | 8.0 | 15.0 |
| Cycle time, min | 16 | 16 | 16 |
| Throughput, L STP/h/kg | 617.87 | 60.907 | 61.688 |
| $H_2$ purity, Step II | 99.999 | 99.998 | 99.858 |
| $H_2$ purity, Step III | 99.994 | 99.071 | 98.120 |
| $H_2$ recovery | 28.927 | 55.482 | 89.676 |
| CO purity, Step IV | 90.689 | 94.222 | 97.936 |
| CO recovery | 99.908 | 98.363 | 95.734 |

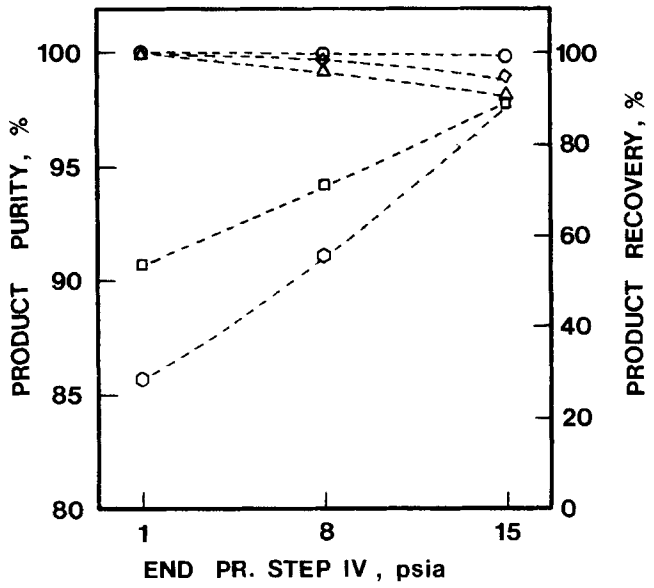


FIG. 6. Effects of end pressure of countercurrent evacuation step on PSA separation (predicted). (●) $H_2$ purity Step II, (▲) $H_2$ purity Step III, (■) CO purity Step IV, (⬢) $H_2$ recovery, (♦) CO recovery.



## Effects of Cycle Time

Three runs (Runs I, H, and C) were made to study the effects of cycle time when the other parameters were fixed. Cycle time was the time during which the adsorber went through all four steps and returned to its original conditions. The effects of cycle time (with other conditions fixed) can be discussed by bed utilization. A shorter cycle time corresponds to a lower bed utilization, which results in higher purity of the lighter component product and lower recovery of the same component. Runs I, H, and C are compared in Table 4 and Fig. 7. For Runs I and H the cycle time was defined as four times the step time (Steps I, II, and III were of same length of time), though Step IV for these two runs was 4 min due to limitation of the pumping capacity. It took approximately 4 min for the pump used in our experiments to evacuate the column to 1.0 psia. In modeling studies, however, a Step IV time of 2 and 3 min was used for Runs I and H, respectively. Table 4 and Fig. 7 show that the purities and recoveries of both components are sensitive to cycle time. An increase in cycle time lowered the $H_2$ purity. On the other hand, it increased the $H_2$

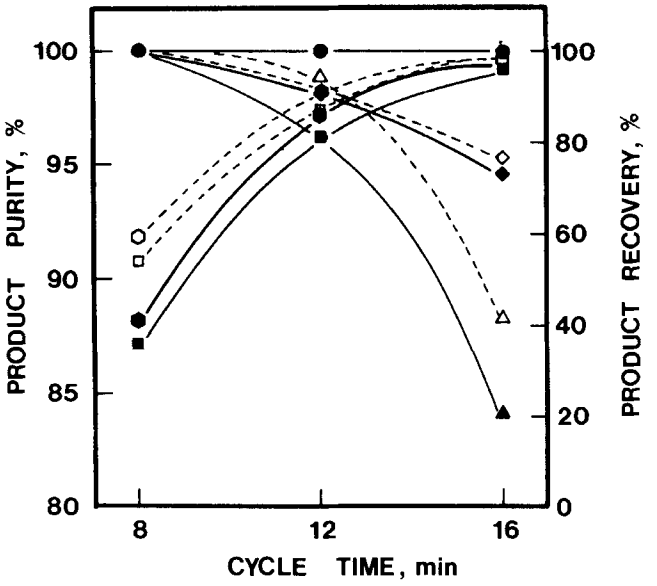


FIG. 7. Effects of cycle time at constant throughput on PSA separation. (●) $H_2$ purity Step II, (▲) $H_2$ purity Step III, (■) CO purity Step IV, (⬢) $H_2$ recovery, (♦) CO recovery. Solid line: experimental. Dashed line: predicted.



recovery and also increased the CO product purity. However, CO purity and $H_2$ recovery both tended to level off with an increase in cycle time. A cycle time above 16 min (4 min for each step) is probably not desirable because the change in $H_2$ recovery and CO purity would insignificant compared to the decrease in $H_2$ purity. The effect of cycle time was discussed qualitatively by Doshi et al. (*13*). They also discussed the economic aspects of the optimization of cycle time for a PSA process.

### Effects of Ambient Temperature

Commercial PSA processes operate under different ambient conditions. Therefore, a practical question arises about the possible effects of ambient temperature on the performance of PSA processes. The adsorbers are operated at nearly adiabatic conditions in commercial operation, so the only possible effect will be due to the temperatures of the influent streams (feed, repressurization $H_2$), which will be close to ambient temperature (if there is no preheating or precooling of these

streams). Three modeling runs (Runs O, P, and Q) were made to see the effects of ambient temperature. In the model, however, heat transfer with the surroundings was taken into account because bed size was small. According to Table 6, a higher ambient temperature gives better separation for a hydrogen-lean feed mixture. This is probably due to the fact that for such mixtures the purity of the lighter component depends on the degree of bed cleaning at the end of the cycle (at the end of Step IV), and a higher temperature would help desorb the CO in the column in Step IV. In the literature (*10*, *13*), however, it was reported that lower temperatures are favorable for better separation, but it should be noted that both studies in the literature were done for $H_2$-rich mixtures. Their authors concluded that lower temperature increases the adsorption capacity and consequently results in lower bed utilization (for the same feed rate) and higher $H_2$ purity.

Three more runs (Runs R, S, and T) were made for a 20/80 $CO/H_2$ mixture ($H_2$ rich). The throughput was increased and again the temperature was varied from 5 to 35°C. This time the effects were in agreement with the literature studies. This shows that the effect of ambient temperature also depends on the feed mixture (the extent of impurity). If the goal is to get a high purity lighter component product, then higher ambient temperature is good for lean feed mixtures with that component and vice versa. The argument can be used for preheating and precooling of gases (feed and repressurization $H_2$). The preheating of gases should



TABLE 6
Effects of Ambient Temperature on PSA Separation

| | Run | | | | | |
|---|---|---|---|---|---|---|
| | O | P | Q | R | S | T |
| Feed composition | 20/80 $H_2/CO$ | | | 20/80 $CO/H_2$ | | |
| Feed pressure, psia | 314.7 | | | 314.7 | | |
| End pressure, Step III, psia | 14.7 | | | 14.7 | | |
| End pressure, Step IV, psia | 1.0 | | | 1.0 | | |
| Cycle time, min | 16 | | | 16 | | |
| Ambient temperature °C | 5 | 20 | 35 | 5 | 20 | 35 |
| Throughput, L STP/h/kg | 58.394 | 58.367 | 58.376 | 169.900 | 169.570 | 169.158 |
| $H_2$ purity, Step II | 99.999 | 99.999 | 99.999 | 99.987 | 99.987 | 99.987 |
| $H_2$ purity, Step III | 87.962 | 88.363 | 88.569 | 90.943 | 90.817 | 90.727 |
| $H_2$ recovery | 97.712 | 97.665 | 97.619 | 99.784 | 99.865 | 99.974 |
| CO purity | 99.716 | 99.697 | 99.694 | 99.025 | 98.933 | 98.819 |
| CO recovery | 76.489 | 76.547 | 76.754 | 87.751 | 97.928 | 96.606 |

improve the purity of the lighter product for a lean mixture with the lighter component.

From the above discussion on the effects of different process variables on process performance, it is clear that optimum values of these parameters should be chosen depending on the separation requirement. Also, the optimization of these parameters should involve the economic aspects to ascertain the commercial potential of this process.

## Cycle Improvement with the Addition of a New Step

As discussed before, the main reason for replacing the purge step (from a conventional 5-step cycle) with the evacuation step was for $H_2$ recovery. The purge step (at nearly atmospheric pressure) consumed a significant fraction of the amount of $H_2$ in the feed (for our feed mixture) to produce a high-purity $H_2$ product in Step II. However, according to the literature (*2*, *10*), the purge step improved $H_2$ purity for $H_2$-rich feed mixtures, so a new vacuum purge step was investigated. This step involved purge of the bed with $H_2$ during evacuation, when the pressure of the bed was already low. Due to the low pressure, the amount of $H_2$ used in this step was very small. The cycle sequence for this new cycle was:

| | |
|---|---|
| Step I: | $H_2$ pressurization (4 min). |
| Step II: | High-pressure adsorption (4 min) |
| Step III: | Cocurrent depressurization (4 min) |
| Step IVa: | Countercurrent evacuation (2 min) |
| Step IVb: | Vacuum purge (2 min) |

The experimental set-up and procedure were similar to that described earlier. The purge was started after a 2-min evacuation step, and the evacuation continued from the feed end of the column while the purge was on.

Three runs (Runs C, J, and K) were performed to study the effect of the amount of purge on separation by varying the purge/feed ratio. The purge/feed ratio was defined as the amount of $H_2$ used in the purge step divided by the amount of $H_2$ in the feed in Step II. The results of Runs C, J, and K are compared in Table 4 and Fig. 8. It can be seen that the vacuum purge effectively cleaned the bed and thus increased the $H_2$ product purity. It also stripped the adsorbed CO from the bed and hence increased CO recovery. On the other hand, $H_2$ purge diluted the CO product. The interesting point is that a small amount of purge improved

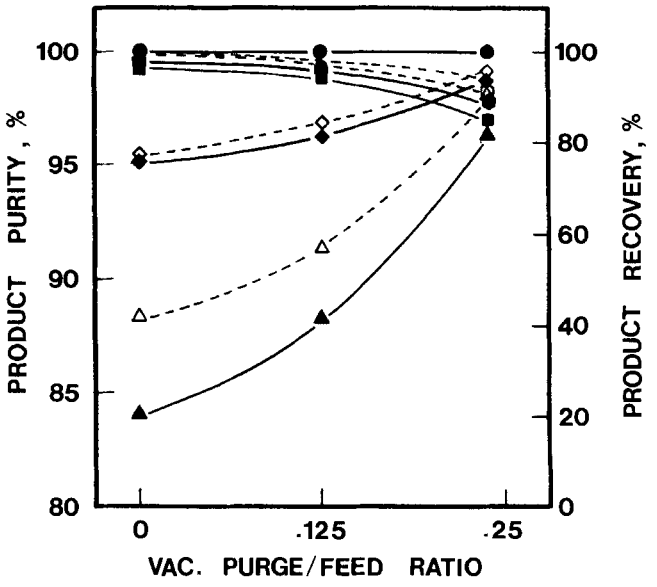


FIG. 8. Effects of vacuum purge on PSA separation. (●) $H_2$ purity Step II, (▲) $H_2$ purity Step III, (■) CO purity Step IV, (⬢) $H_2$ recovery, (♦) CO recovery. Solid line: experimental. Dashed line: predicted.



the $H_2$ product purity without significantly lowering $H_2$ recovery. But if the purge/feed is further increased (from Runs J to K), $H_2$ recovery is also affected. According to Fig. 8, a purge/feed ratio in the range of 0.05 to 0.15 is optimum for the conditions discussed.

The effect of vacuum purge is very similar to the effect of purge (in a conventional 5-step cycle) as reported in the literature (*2*, *3*, *13*).

## CONCLUSIONS

Experimental results showed that high purity hydrogen (99.999% by volume) can be produced from a 20/80 binary mixture of $H_2$/CO by a 4-step PSA using zeolite-5A sorbent.

It was seen that lower throughput, higher feed pressure, higher end pressure of cocurrent depressurization, and lower end pressure of countercurrent evacuation increased the $H_2$ product purity. Hydrogen product purity and recovery were very sensitive to cycle time (For equal-time steps). A shorter cycle produced higher $H_2$ purity but lowered the $H_2$ recovery.

The ambient temperature had an interesting effect on separation. It was found that higher ambient temperature was desirable for a $H_2$ lean feed mixture, and vice versa.

A new PSA cycle step, "vacuum purge," was investigated. The separation ($H_2$ purity) can be improved by this step without significantly lowering $H_2$ recovery if small amounts of purge are used. An equilibrium model which successfully predicted all effects was developed.

## SYMBOLS

| | |
|---|---|
| $A, B, C, D$ | constants in heat capacity equation |
| $a, b, c, d$ | parameters for LRC equation |
| $C$ | gas phase concentration (mol/m$^3$) |
| $C_p$ | heat capacity of gas (cal/mol/K) |
| $C_{pa}$ | heat capacity of adsorbed phase (cal/mol/K) |
| $C_{ps}$ | heat capacity of adsorbent (cal/g/K) |
| $C_{pw}$ | heat capacity of wall (cal/g/K) |
| $D$ | axial dispersion coefficient (m$^3$/s) |
| $H$ | heat of adsorption (cal/mol) |
| $h$ | heat transfer coefficient (cal/m$^2$/K/s) |
| $L$ | height of bed (m) |
| $P$ | pressure (atm) |
| $q$ | adsorbate concentration in solid phase (mol/m$^3$) |
| $R$ | gas constant |
| $r$ | radius of column (m) |
| $T$ | temperature (K) |
| $t$ | time (s) |
| $u$ | intersticial velocity (m/s) |
| $x$ | mole fraction in adsorbed phase |
| $y$ | mole fraction in gas phase |
| $z$ | axial position in the bed (m) |

### Greek Symbols

| | |
|---|---|
| $\varepsilon$ | fractional void in the bed |
| $\zeta$ | density |

### Superscript

| | |
|---|---|
| * | equilibrium |

## Subscripts

| | |
|---|---|
| $B$ | bed |
| $f$ | feed |
| $i$ | component $i$ |
| 0 | initial |
| $w$ | wall |

## REFERENCES


1. S. J. Doong and R. T. Yang, *Chem. Eng. Commun.*, In Press.
2. P. L. Cen and R. T. Yang, *Ind. Eng. Chem., Fundam.*, In Press.
3. R. T. Yang and S. J. Doong, *AIChE J., 31,* 1829 (1985).
4. S. J. Doong and R. T. Yang, *Ibid., 32,* 397 (1986).
5. P. C. Wankat, *Large-Scale Adsorption and Chromatography,* CRC Press, Boca Raton, Florida, 1986.
6. P. L. Cen and R. T. Yang, *Sep. Sci. Technol., 20,* 725 (1985).
7. H. W. Haynes Jr., "Heat and Mass Transfer in Packed Bed—I," *AIChE, Modular Instruction Series,* Module E 3.5 (1982).
8. N. S. Raghavan, M. M. Hassan, and D. M. Ruthven, *AIChE J., 31,* 385 (1985).
9. R. T. Yang, *Gas Separation by Adsorption Processes,* Butterworth, Boston, 1987.
10. S. J. Doong and R. T. Yang, *Reactive Polymers,* In Press.
11. D. M. Ruthven, *Principles of Adsorption and Adsorption Processes,* Wiley, New York, 1984.
12. Y. N. Chan, F. B. Hill, and Y. W. Wong, *Chem. Eng. Sci., 36,* 243 (1981).
13. K. J. Doshi, C. H. Katina, and H. A. Stewart, *AIChE Symp. Ser., 67* (1971).
14. R. T. Cassidy and E. S. Holmes, *Ibid., 23* (1983).
15. C. E. Keller, "Industrial Gas Separation," *ACS Symp. Ser., 23* (1983).
16. F. Corr, F. Dropp, and E. Rudelstorfer, *Hydrocarbon Processing,* p. 119 (1979).
17. C. W. Skarstrom, *Ann. N. Y. Acad. Sci., 72,* 751 (1959).
18. S. Sircar, "Air Fractionation by PSA," U.S. Patent 4,329,158 (1982).
19. H. A. Stewart and J. L. Heck, *Chem. Eng. Prog., 65,* 78 (1969).
20. C. W. Skarstrom, "Fractionating Gas Mixtures by Adsorption," U.S. Patent 2,444,627 (1960).


*Received by editor December 22, 1986*
*Revised April 10, 1987*